DOI:10.28974/idojaras.2026.3.4

IDŐJÁRÁS
Quarterly Journal of the HungaroMet Hungarian Meteorological Service
Vol. 130, No. 3, July – September, 2026, pp. 297–315

Some novel observations of terrain-disrupted airflow at the Hong Kong International Airport based on range-height indicator and plan position indicator scans of the LIDAR and their numerical simulations

Yu Ting Leung, Pak Wai Chan*, Man Lok Chong, Chun Kit Ho, Kai Kwong Lai, Ping Cheung, and Yan Yu Leung

Hong Kong Observatory,
134A Nathan Road, Kowloon, Hong Kong, China

**Corresponding author E-mail: pwchan@hko.gov.hk*

(Manuscript received in final form on March 18, 2026)

Abstract— Range-height indicator (RHI) scans from the Doppler Light Detection And Ranging (LIDAR) systems at the Hong Kong International Airport (HKIA) reveal vortices associated with Kelvin-Helmholtz (KH) instability, jump-like features and mountain waves associated with lower kills and a gap on Lantau Island nearby HKIA. These novel features of terrain-disrupted airflow at HKIA that has not been documented before. This paper analyzes such flow features by considering some parameters of the airflow based on the upper air sounding in Hong Kong, such as Richardson number, Scorer parameter, and Froude number. An attempt has also been made to simulate these novel flow phenomena at HKIA using a high resolution mesoscale numerical weather prediction (NWP) model. The modeling results are found to be a mixed success. Some features, such as mountain waves and jump-like feature, are readily reproduced. However, vortices associated with KH instability are difficult to reproduce, and the vortex shedding simulation does not fully reproduce the observational data based on the Doppler LIDARs. The results in this paper are considered to be useful for the study of mountain meteorology in Hong Kong and elsewhere in the world.

Key-words: terrain-disrupted airflow, LIDAR, Hong Kong International Airport

1. *Introduction*

HKIA is located just to the northwest of the mountainous Lantau Island, which has peaks as high as 1000 m above sea level and valleys as low as 300 m in between. In stable boundary layer, various kinds of terrain-disrupted airflow features may occur over the airport area, which may be hazardous to the arriving and departing aircraft due to the creation of low-level windshear and turbulence. The terrain-disrupted airflow features are best captured by the LIDAR systems. Since 2002, LIDARs have been gradually introduced to HKIA to capture the terrain-induced airflow disturbances.

With the deployment of more LIDAR units at the airport, different scanning strategies could be implemented to these instruments and recently both plan position indicator (PPI) and range height indicator (RHI) scans of the LIDARs are available every several minutes, in addition to the glide path scans that are primarily used to build up the headwind profiles to be encountered by the aircraft and to alert low-level windshear. In this paper, some novel LIDAR observations of wind features, including vortices associated with KH instability, would be presented, analyzed, and discussed, through depiction of the corresponding LIDAR velocity scans and calculation of atmospheric parameters such as Richardson number based on profiling data. Moreover, an attempt is made to simulate these features using a high resolution mesoscale numerical weather prediction model at large eddy simulation mode, with a spatial resolution as small as 40 metres.

This paper are believed to be useful for studying mountain meteorology in Hong Kong and elsewhere in the world, through documentation of the LIDAR observation, analysis of atmospheric profile, and discussion of numerical simulation. As such, the results in the paper are of academic interest. At the same time, though no windshear or turbulence reports are obtained in these cases, the novel flow features are also considered to be of practical importance as they may lead to fluctuations of the airflow to be encountered by the aircrafts in an operating airport.

2. *Materials and methods*

2.1. Meteorological instrumentation

The major meteorological instrument considered in this paper is the Doppler LIDAR. There is runway specific LIDAR installation at HKIA, i.e., one LIDAR is installed near the centre of each of the three parallel runways of the airport. In this paper, the scans from the LIDAR at the second runway, i.e., HKG2 LIDAR, and the LIDAR at the third (or north) runway, i.e., HKG3S LIDAR, would be considered. The LIDARs are so-called long-range units, providing spatial coverage up to 10 to 15 km from the equipment itself. They work with laser beams with wavelengths of about 1.5 microns, and measure the line-of-sight velocities by tracking the movement of the aerosols in the air. The accuracy of wind measurement is in the order of 1 m/s or less.

These LIDARs provide plan position indicator (PPI) scans at a number of elevation angles in order to give an overview of the wind distribution inside and around the airport. They also make a number of range height indicator (RHI) scans at selected azimuth angles from the north to capture the vertical structure of the airflow, e.g. along the runway glide paths, or in the planes perpendicular to the major mountain features of Lantau Island, such as downstream of the hills and the valleys. The PPI and RHI scans are updated every few minutes. Only the Doppler velocity images would be considered, which provide the line-of-sight velocities for monitoring low-level jets, waves and jump-like features in the RHI scans, and vortices in both RHI and PPI scans.

The background meteorological conditions are provided by the radiosonde ascent data at King's Park, which is located at about 60 km to the east of the airport. Inside HKIA itself, vertical profiles of the wind are also provided every 10 minutes by the radar wind profiler running at 1290 MHz radar waves, and vertical profiles of temperature and humidity are provided hourly by the ground-based microwave radiometer at the airport, which works with 7 oxygen channels and 7 water vapour channels. Compared with radiosonde, wind profilers and radiometers have coarser vertical resolutions, but much higher temporal resolutions. These vertical profiles are used to calculate the various parameters such as Richardson number, Froude number, Scorer parameter, etc.

2.2. Numerical model

The mesoscale model in use is the Regional Atmospheric Modeling System (RAMS) version 6.3. Its initial and boundary conditions are provided by the re-analysis of European Centre for Medium Range Weather Forecast (ECMWF) at a spatial resolution of 25 km and a temporal resolution of every hour. The spatial resolution of the RAMS simulation is increased by a factor of five, namely, 25 km, 5km, 1 km, 200 m, and 40 m. The coarse domain has a timestep of 10 seconds, with a timestep ratio of 10. The first model level is about 30 m above sea surface. There is then stretching ratio of 1.08 (i.e., the ratio of the model level heights between the adjacent model levels). The simulation is essentially a large eddy simulation (LES) of terrain-disrupted airflow at HKIA.

Of particular importance is the choice of turbulence parameterization schemes. The Smagorinsky scheme (*Smagorinsky*, 1963) is employed for the first two nests, and the Deardorff scheme (*Deardorff*, 1980) for the remaining three nests. The sensitivity of the simulation results to the choice of turbulence parameterization schemes would be considered in a follow-up study. The existing combination is found to produce reasonable results in the past studies of terrain-induced windshear at HKIA. The other physical settings could be found in *Chan et al.* (2021).

3. Results

3.1. Kelvin-Helmholtz (KH) instability

Synoptically, a ridge of high pressure over southeastern coast of China brought easterly winds to the coast of Guangdong on that day (not shown). For the RHI scan of HKG2 LIDAR to the west-southwest, outbound easterly flow was measured within the atmospheric boundary layer. However, the easterly winds were not static and waves could be identified at various heights (*Fig. 1*).

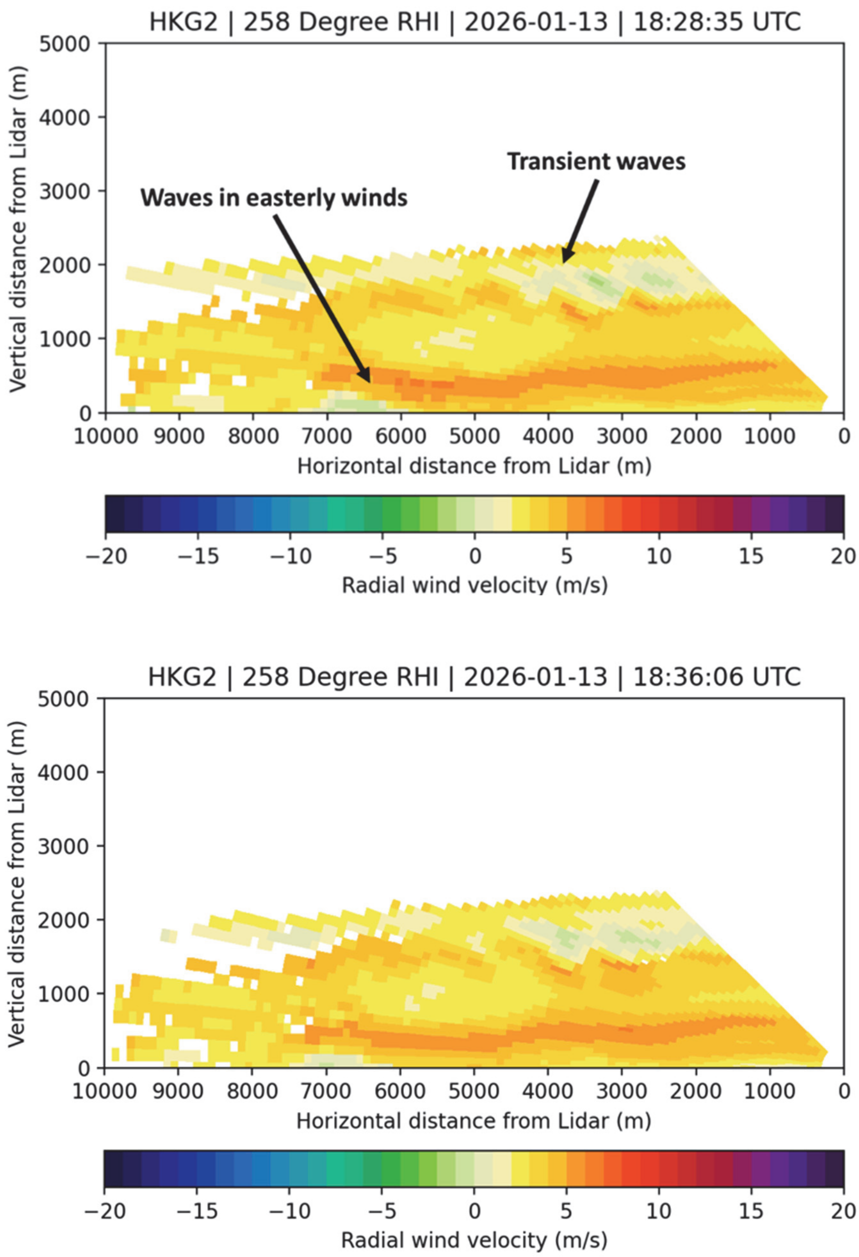

Fig. 1. RHI scans of Doppler velocity of HKG2 LIDAR, showing the vortices associated with KH instability at two time instances (a) and (b).

A number of waves was found in the easterly wind between the ground and about 1000 m above ground. At higher altitudes, between about 1000 m and 2000 m above ground, not only transient waves occurred, some inbound flow could be identified above the waves, so that there was a number of vertical circulating flow with a size of about several hundred metres. This is the first documented observation of waves associated with KH instability in the RHI scans of the Doppler LIDARs at HKIA. Such waves related to KH instability occurred for a few minutes only in the RHI scans and disappeared afterwards.

To study the KH instability further, the wind data from the radar wind profiler and the temperature profiles from the ground-based microwave radiometer at the airport are analyzed in detail with the calculation of Richardson number (*Ri*). Hourly *Ri* is determined from the following equation:

$$Ri = \frac{N^2}{\left(\frac{\partial u^2}{\partial z}\right)+\left(\frac{\partial v^2}{\partial z}\right)} \quad (1)$$

where *N* is the Brunt-Vaisala frequency, *u* and *v* are the horizontal components of the wind, and *z* is the height. It is a ratio of the buoyancy term and the shear force team. The vertical wind profile from the high mode of the wind profiler (with a nominal measurement height of 6 km above ground) is considered.

The vertical profiles of the Richardson number at 18 UTC and 19 UTC of January 13, 2026 are considered, as shown in *Fig. 2(a)*. In this period, *Ri* decreased from 0.82 to 0.18 at a height of about 1500 m above ground. Further analysis of the two terms (*Figs 2(b)* and *2(c)*) shows that, while there was a 7% decrease of the buoyancy term, there was a 320% decrease of the shear force term. As a result, *Ri* is less than 0.25 for a short while, which is consistent with the occurrence of KH instability as in the RHI scan of the LIDAR.

To study the significant drop of shear force term in detail, the time-height cross section of the wind as measured by the radar wind profiler is shown in *Fig. 3*. At 18 UTC, the 10-minute wind direction/wind speed at 1400 m is 120 degrees / 5.3 m/s, and at 1500m is 127 degrees / 6.1 m/s. At 19 UTC, the 10-minute wind direction/wind speed at 1400 m is 133 degrees / 4.8 m/s, and at 1500 m is 160 degrees / 4.4 m/s. The wind direction angle difference between 1400 m and 1500 m changes from 7 degrees to 27 degrees. The 320% increase of shear force term is related to a quite small angle difference from 18 UTC to 19 UTC. It is shown in *Fig.3* that such a change happens for a short while, which is consistent with the observed transiency of the occurrence of KH instability wave in the RHI scans of the LIDAR. The slight change of the wind direction angle difference is believed to be correct.

An attempt is made to simulate the waves associated with the KH instability, namely, initialized at 17 UTC of January 13, 2026, running up to January 20, 2026. Within the generally outbound flow below a height of about 2500 m above ground, some isolated areas of inbound flow could be simulated (*Fig.4*), which seems to be consistent with the actual LIDAR observation (*Fig.1*). However, the wave features are not apparent in the simulation. Similar to the actual RHI scans of the LIDAR, such inbound flow regions are transient and occurs for a few minutes only (not shown).

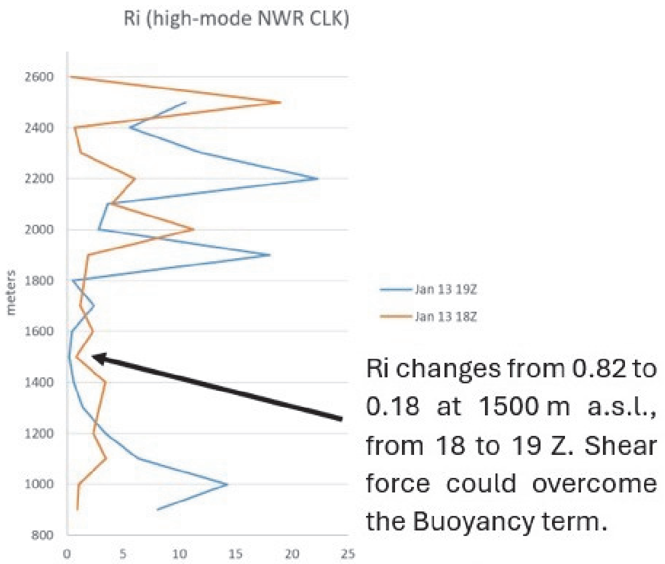

(a)

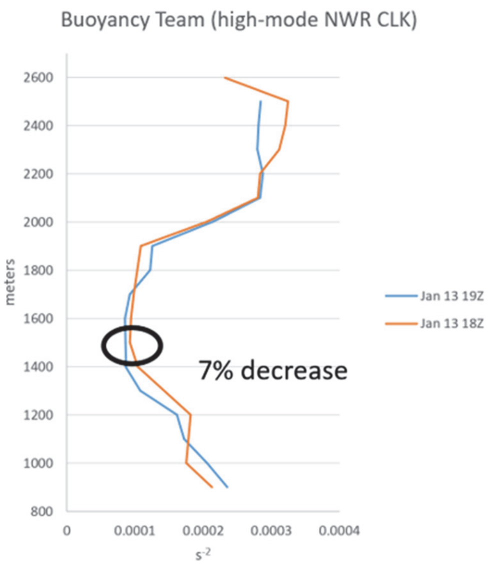

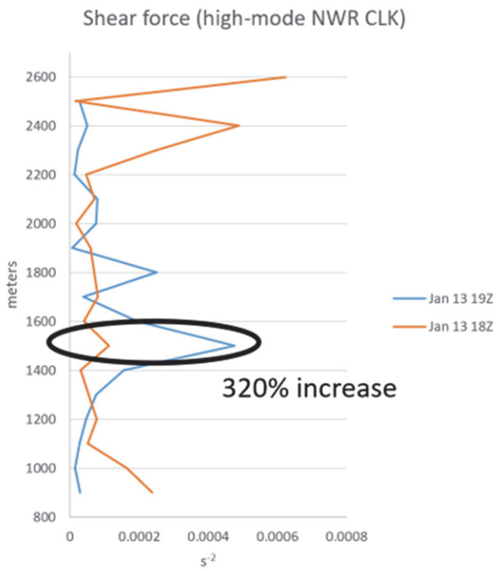

(b) (c)

Fig. 2. Vertical profile of Richardson number (a), and the vertical profiles of buoyancy term (b) and shear force term (c).

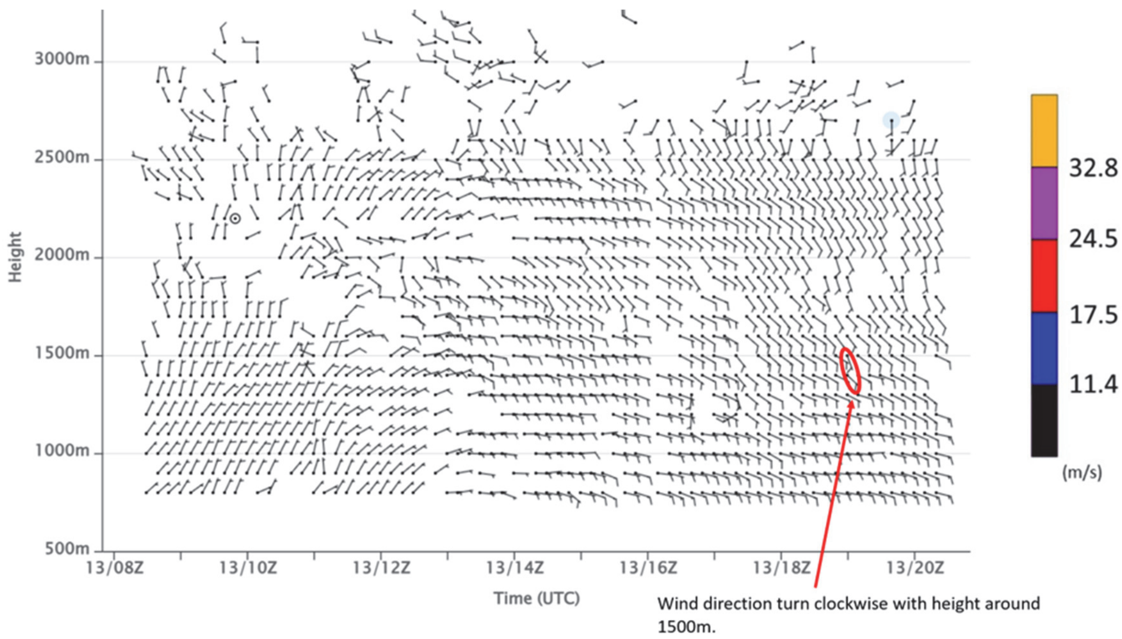

Fig.3. Time-height cross section of horizontal winds from the wind profiler at the airport.

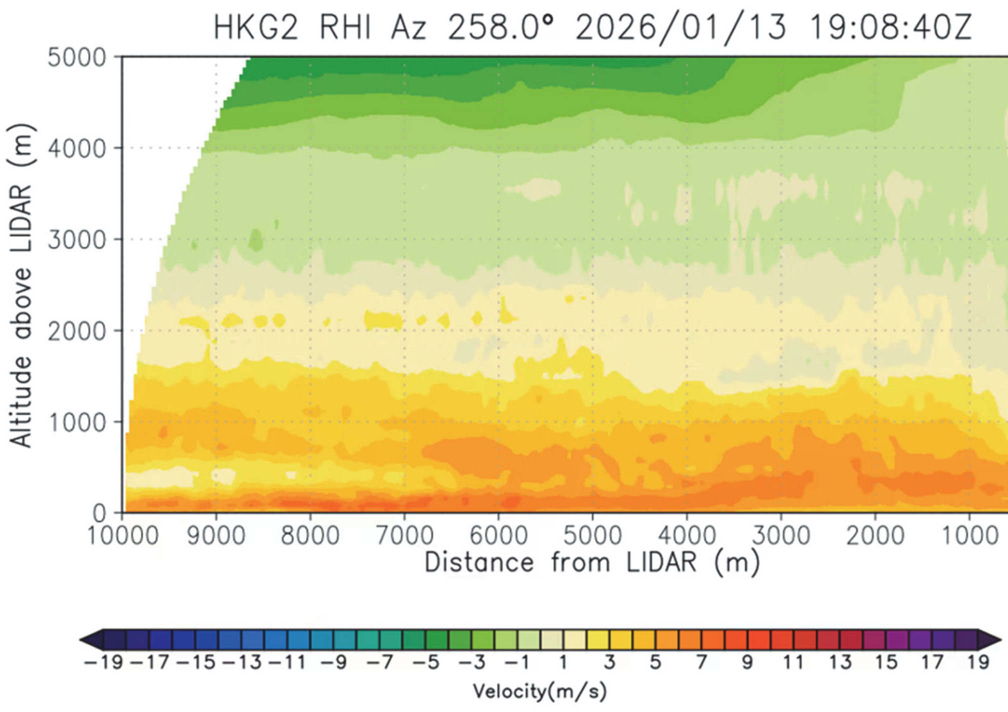

Fig. 4. Simulated RHI scan of Doppler velocity of HKG2 LIDAR.

3.2. Vortex-shedding

As shown by the PPI scans of the LIDAR, fresh to strong east to southeasterly winds prevailed over the airport region at the night time of December 21, 2025. To the southwest of the airport, the east-southeasterly flow was disrupted by the mountains of Lantau Island, leading to the occurrence of shedding vortices from the terrain. Such vortices appear as inbound flow (coloured green) in the LIDAR's PPI scan. A sequence of the event is shown in *Fig. 5*, with the vortex appearing to detach from the mountain first (*Fig.5(a)*), travelling downstream (*Fig.5(b)*), getting to the maximum range of the LIDAR (*Fig.5(c)*) and dissipating gradually, with the occurrence of another shedding vortex from the mountain (*Fig.5(d)*). The whole process takes about 20 minutes.

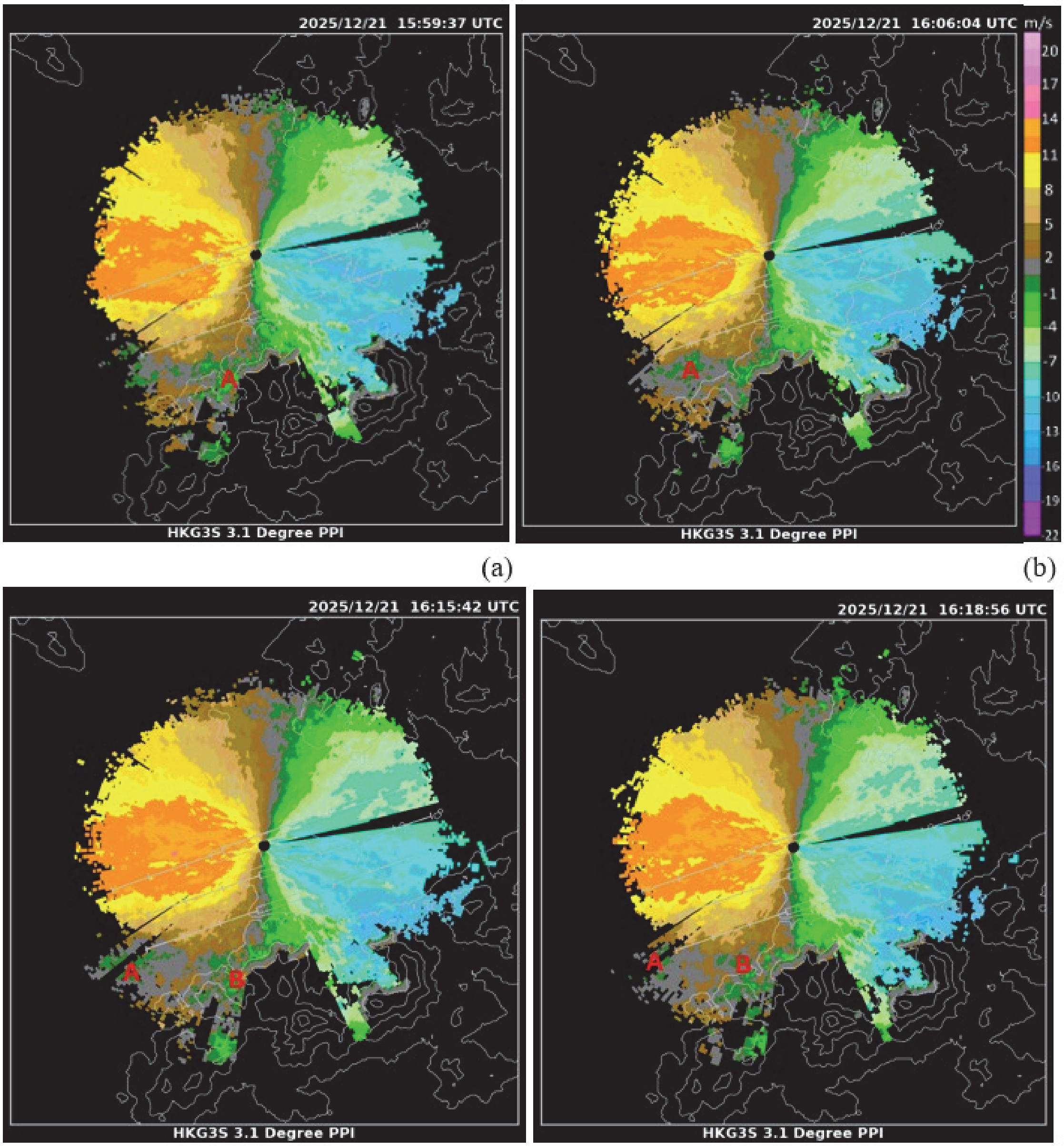

(a) (b)

(c) (d)

Fig.5. PPI scan of Doppler velocity of HKG3S LIDAR, showing shedding of vorices.

In order to study the period of shedding vortices, the associated with direction changes as measured by the anemometer at the western end of the south runway (R1W anemometer) have been analyzed using Fourier transform. The period from 18 UTC of December 21, 2025 to 05 UTC of December 22, 2025 is analyzed, and the wind data are considered in a number of half-an-hour time intervals. Within each half an hour, the 1-minute mean wind direction from R1W anemometer updated every minute is used to build up the time series, which is analyzed through Fourier transform. A typical frequency spectrum is shown in *Fig. 6(a)*. There are a number of peaks identified in the spectrum, and the most prominent peak has been selected to plot the time series of the most prominent periods of fluctuations of wind direction as shown in *Fig. 6(b)*. The major periods are around 20 minutes at 18 UTC of December 21, 2025, 24 minutes at around 22 UTC of that day, and 17 minutes at around 02 UTC of December 22, 2025.

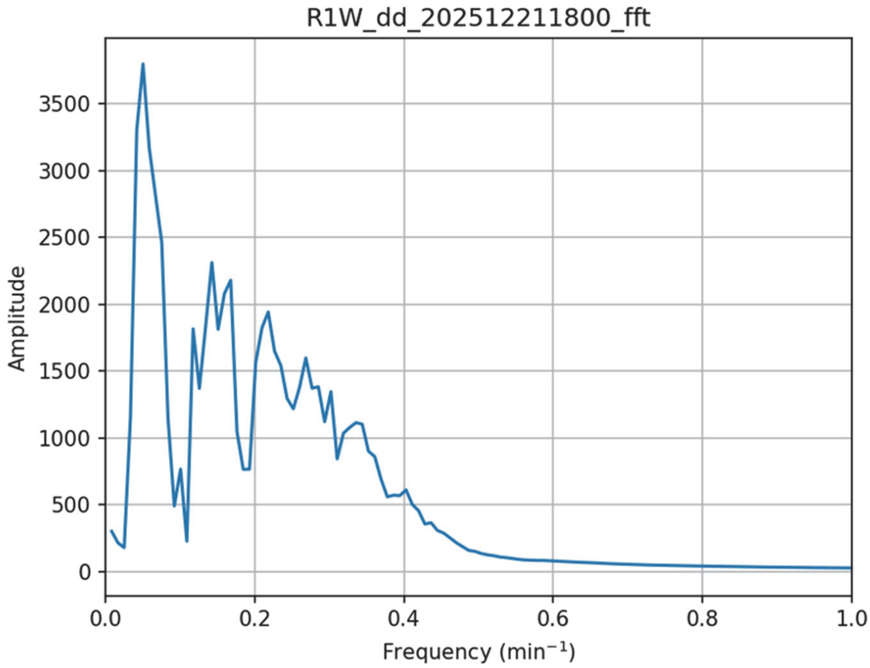

(a)

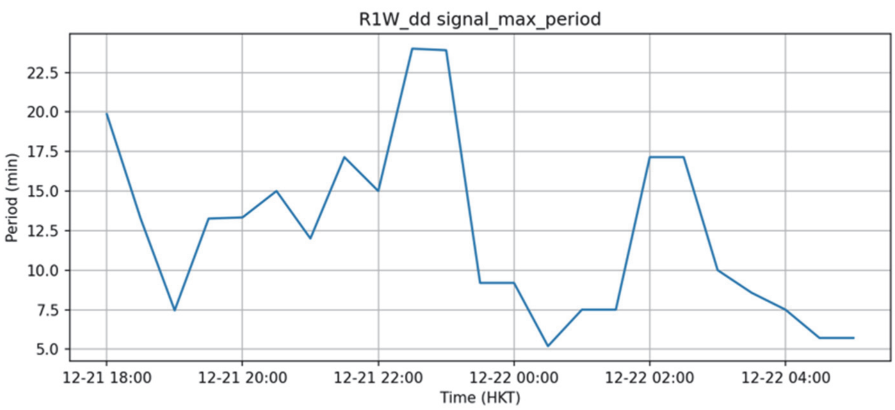

(b)

Fig.6. A sample frequency spectrum of R1W wind direction (a) and the time series of the most prominent period through spectral analysis (b).

When winds blow along a mechanical obstacle such as mountains, oscillatory flow could be observed downstream in the form of vortex shedding when the boundary layer profile is sufficiently stable. According to *Atkinson* (1981), the shedding period T (s) could be expressed in terms of the Strouhal number (S_t) and the horizontal dimension D of the obstacle:

$$T = \frac{D}{S_t U_0}, \tag{2}$$

where U_0 is the background wind speed (m/s) at Nei Lak Shan (747m above sea level), D would be taken as 4000m for Nei Lak Shan as an estimated width of the obstacle for the interest of this study. Based on the above discussion, T ranges about 17 minutes and 24 minutes. U_0 in the order of 8 m/s. As such, S_t is about 0.49 and 0.34. *Atkinson* (1981) suggested that the range of value of S_t would fall within 0.15 to 0.32, which is generally consistent with the observed results.

Vosper (2000) mentioned that the vortex shedding would occur when Froude number (F_h) is less than or equal to 0.4, F_h is defined by:

$$F_h = \frac{U}{Nh} \tag{3}$$

where N is the Brunt–Väisälä frequency (s^{-1}) and h is the height of mountain. U is taken to be about 8 m/s and N is taken to be about the square root of 0.0003 based on radiosonde ascent at King's Park at 13 UTC of December 21, 2025. As such, F_h is found to be about 0.6.

Another formulation of Froude number is based on *White* (1999). The Froude number (Fr) is take to be:

$$Fr = \frac{\langle U \rangle_h}{\sqrt{g_r h}} \tag{4}$$

where $\langle X \rangle$ indicates a vertical/depth average over the extent of X, U is the wind speed, and g_r the reduced gravity, and

$$g_r = \frac{g(\theta_T - \langle \theta \rangle_h)}{\langle \theta \rangle_h} \tag{5}$$

where g is the gravitational constant, θ_T the free troposphere potential temperature, and θ the potential temperature. Based on the radiosonde data at 13 UTC of December 21, 2025, θ_T is about 301 K, and $\langle \theta \rangle_h$ is about 292 K. The wind speed U is about 8 m/s at the mountain top. As such, the Froude number is 0.52.

From the above results, both formulations of Froude number give comparable values. The calculated Froude numbers are generally consistent with the result in *Vosper* (2000).

Numerical simulation has been performed between 14 and 17 UTC of December 21, 2025. A sample sequence of simulated LIDAR PPI scans of Doppler velocity is shown in *Fig. 7*. Vortex shedding has been simulated successfully, and the shedding period is also found to be in the order of around 20 minutes, consistent with the actual observations from the LIDAR.

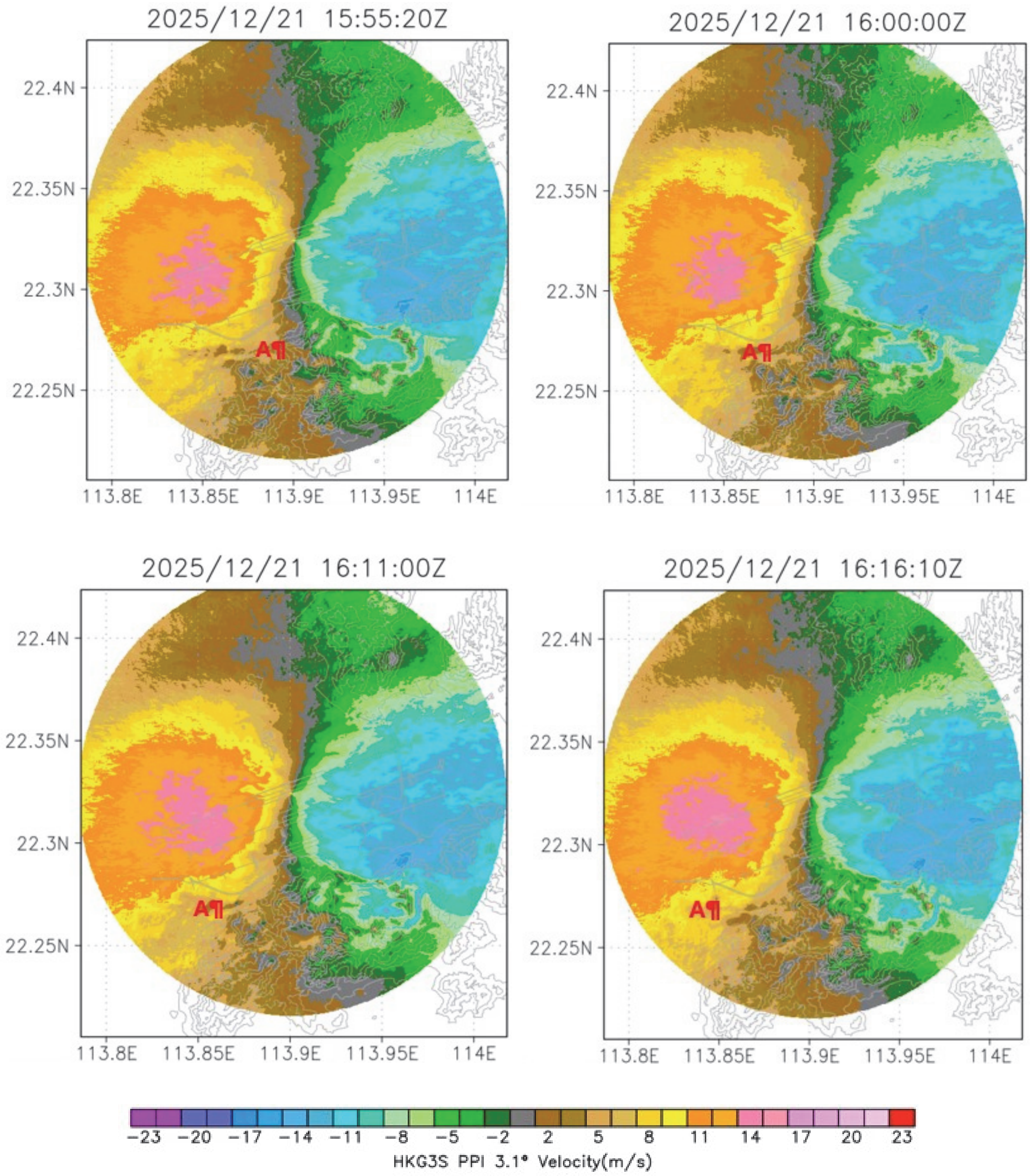

Fig. 7. Simulated PPI scans of Doppler velocity of HKG3S LIDAR, showing the vortex.

3.3. Hydraulic jump and mountain wave

Jump-like feature has been observed in easterly winds flowing over Lo Fu Tau, a hill of about 460 m above sea level at the northeastern part of Lantau Island, as shown in the RHI scan of HKG2 LIDAR with an azimuth angle of 95 degrees (*Fig. 8(a)*). Recirculating flow (inbound flow) has been observed both below and above the easterly jet (coloured dark blue and green), which is a typical feature of jump-like feature.

The jump-like structure is studied further using a two-layer model. The depth of the atmospheric boundary layer, h, can be of the order of the terrain elevation, i.e., 460 m, and the nature of the flow depends upon the Froude number (Fr) in Eq. (4). Based on the radiosonde data at 00 UTC of January 25, 2026, θ_T is about 293 K, and $\langle\theta\rangle_h$ is about 288 K. The wind speed U is about 10 m/s at the mountain top. As such, the Froude number is more than 1, i.e., it is supercritical, and this supports the occurrence of the jump-like feature.

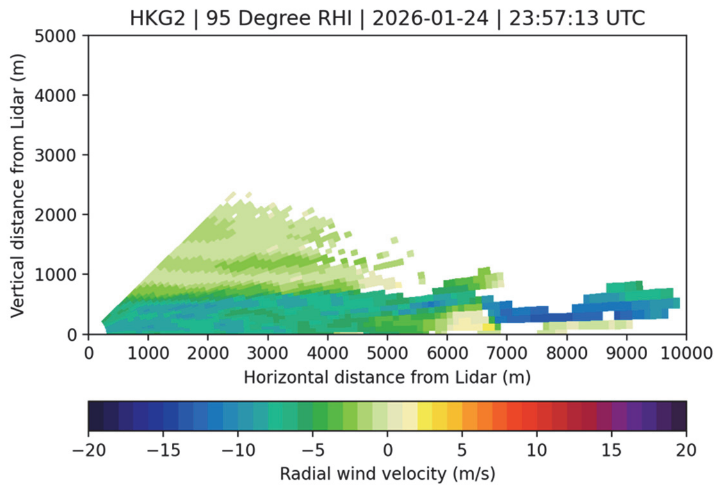

(a)

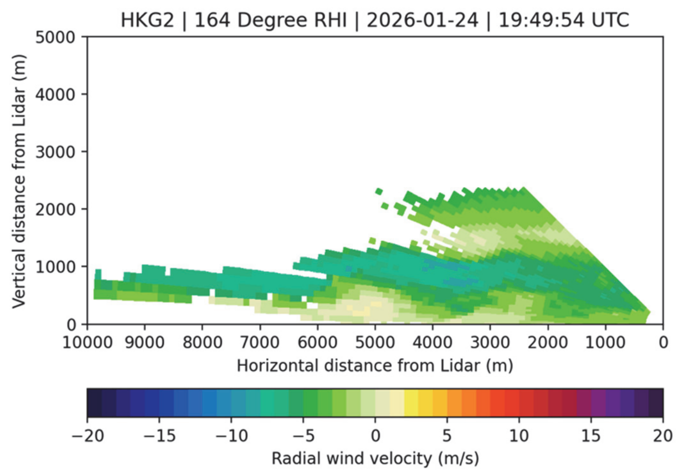

(b)

Fig. 8. RHI scans of HKG2 LIDAR, showing jump-like feature (a) and mountain wave (b).

At the same time, across the Tung Chung gap (a gap of about 300 m above sea level at the middle of Lantau Island), some transient waves have been observed in the RHI scan of HKG2 LIDAR with an azimuth angle of 164 degrees. An example is shown in *Fig. 8(b)*. Recirculating (inbound) flow has been observed below the jet associated with the wave. The wave is transient and occurs for a couple of scans only separated by a few minutes, and disappears afterwards.

In order to study the wave, the Scorer parameter is calculated (*Scorer,* 1949) based on the radiosonde data at 00 UTC of January 25, 2026, as shown in *Fig. 9*:

$$l^2 = (N(z) / U(z))^2 - U_{zz}/U, \tag{6}$$

where N is the Brunt-Vaisala frequency, $U(z)$ is the cross-mountain wind speed profile and U_{zz} is the second derivative of U with height z. The Scorer parameter does not show decreasing trend from ground up to a height of about 700 m above ground. As such, the background atmosphere does not seem to support stationary mountain wave, which is consistent with the rather transient nature of the wave as observed in the 164-degree RHI scan of the LIDAR.

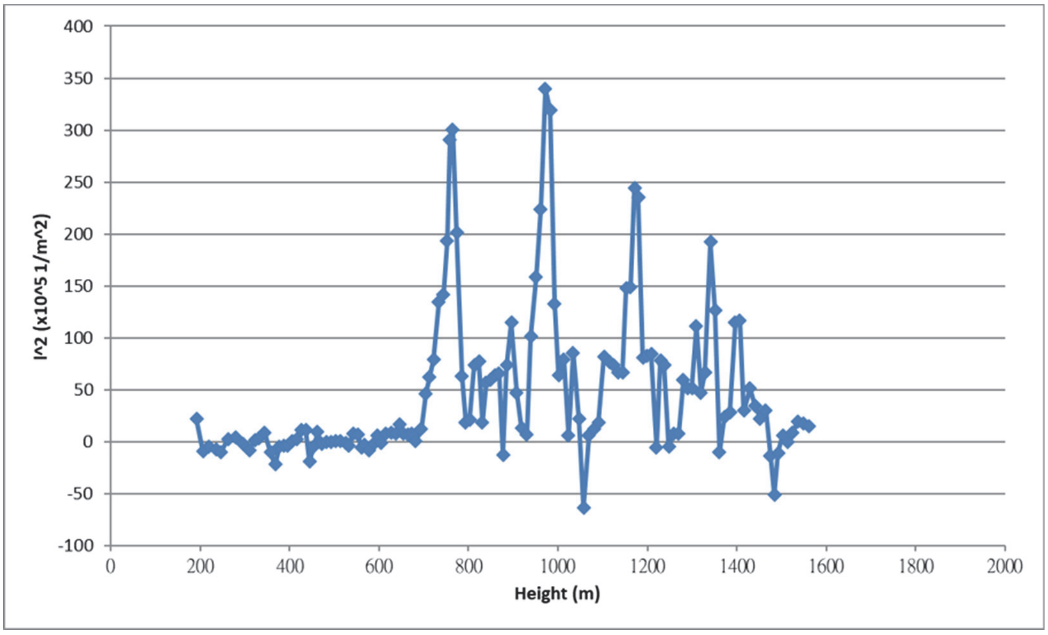

Fig.9. Scorer parameter profile based on radiosonde data for the case of *Fig. 8*.

Numerical simulation has been performed between 18 UTC of January 24, 2026 up to 01 UTC of January 25, 2026. It is very hard to look for jump-like feature at Lo Fu Tau and wave like feature at Tung Chung gap with recirculating flow. A couple of sample simulated RHI scans showing similar features could be found in *Figs 10(a)* and *10(b)*, respectively. In *Fig. 10(a)*, there is a bit of jump-like feature downstream of Lo Fu Tau, with recirculating flow above and below the jet, but the feature lasts for a few minutes only. Similar transiency in wave-like feature is also found in Tung Chung gap in *Figure 10(b)*, with the occurrence of inbound flow below the wave for a short while.

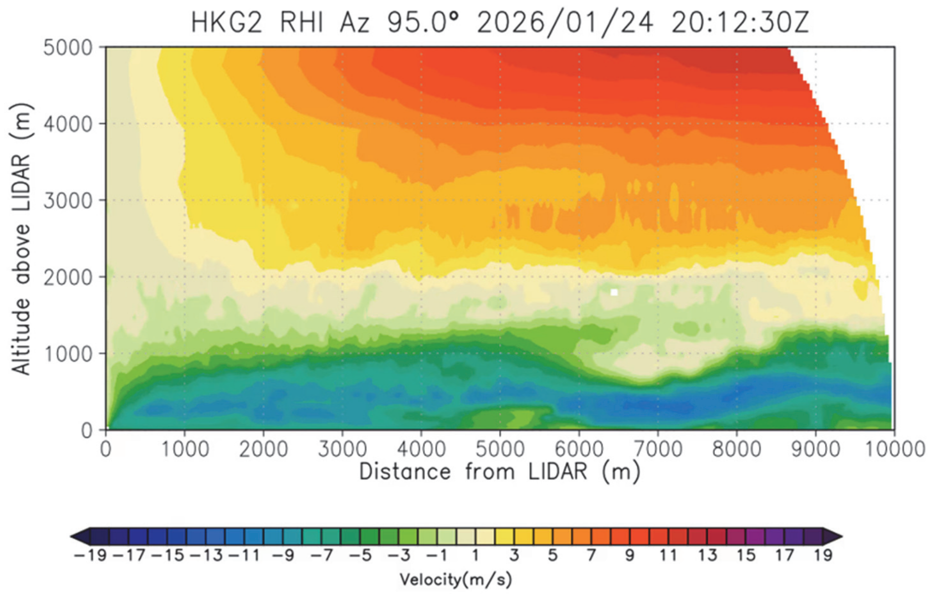

(a)

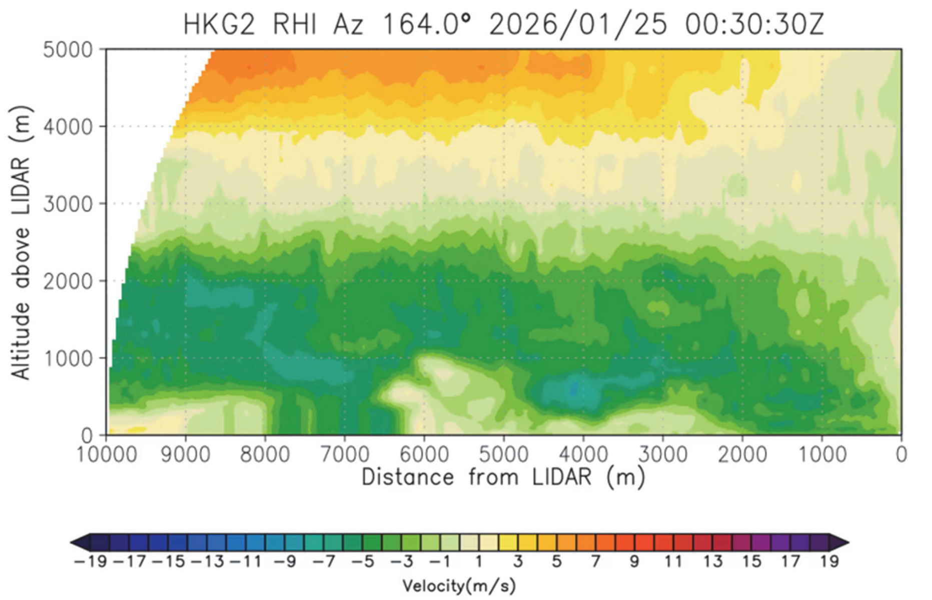

(b)

Fig.10. Simulated RHI scans of HKG2 LIDAR for jump-like feature (a) and mountain wave (b).

3.4. *Mountain wave*

Rather stationary mountain waves are occasionally observed downstream of Lo Fu Tau in easterly winds. An example is shown in *Fig. 11(a)* with a wavelength of about 3000 m. At the same time, a wave could be identified downstream of Tung Chung gap near the airport, as shown in *Fig. 11(b).* Such features normally occur in stable boundary layer, when mountain wake is observed downstream of the mountains of Lantau Island, as shown in the LIDAR PPI scan in *Fig. 12*. There is a west-northwest to east-southeast oriented and elongated flow of inbound velocity (green color) to the west of Lantau Island and southwest of the airport.

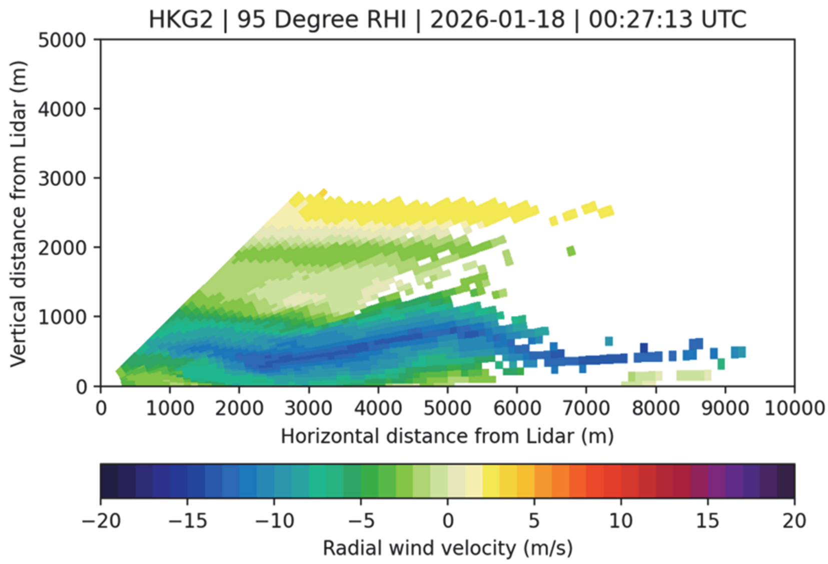

(a)

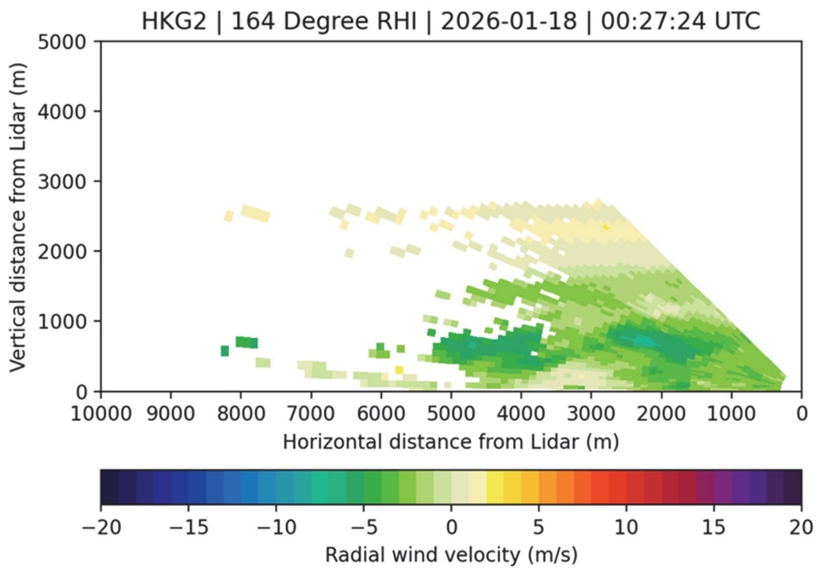

(b)

Fig.11. RHI scans of HKG2 LIDAR showing mountain waves at Lo Fu Tau (a) and the Tung Chung gap (b).

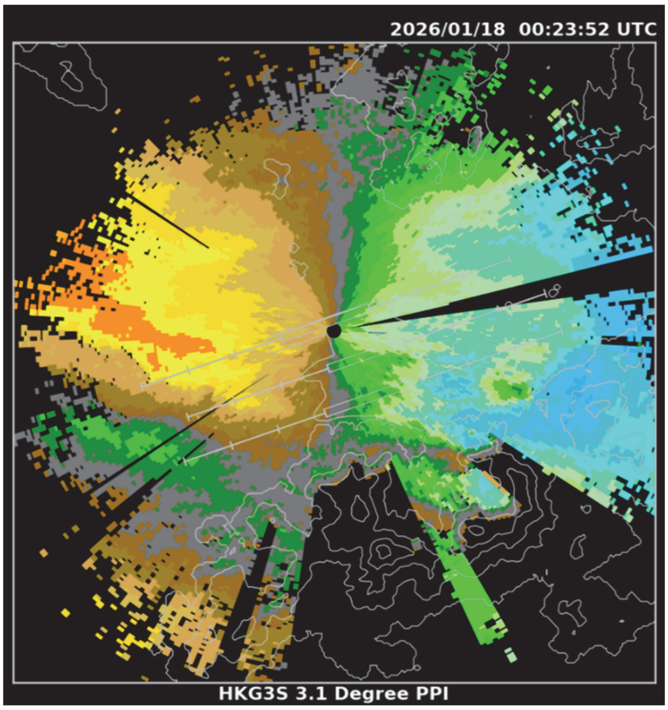

Fig. 12. PPI scan of the LIDAR from HKG3S LIDAR.

Following Eq.(6), the Scorer parameter is calculated based on radiosonde data at King Park at 00 UTC of January 18, 2026. The result is shown in *Fig. 13(a)*. There is a drop of Scorer parameter from a height of about 100 m to about 500 m, which is consistent with the observed mountain wave across Tung Chung gap. On the other hand, the drop of Scorer parameter from 500 m to 800 m is not very clear. From the vertical profile of potential temperature (*Fig. 13(b)*), there is a rather significant temperature inversion at a height of about 600 m above sea level. This strong inversion is favourable to the occurrence of mountain wave. It is consistent with the observed occurrence of stationary mountain wave downstream of Lo Fu Tau with a height of about 460 m above sea level.

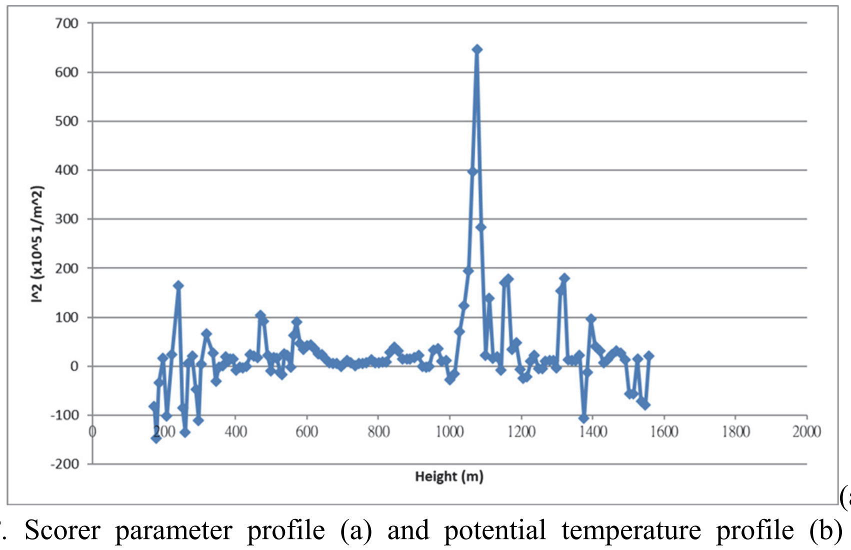

(a)

Fig. 13. Scorer parameter profile (a) and potential temperature profile (b) based on radiosonde data for Lo Fu Tau and the Tung Chung gap.

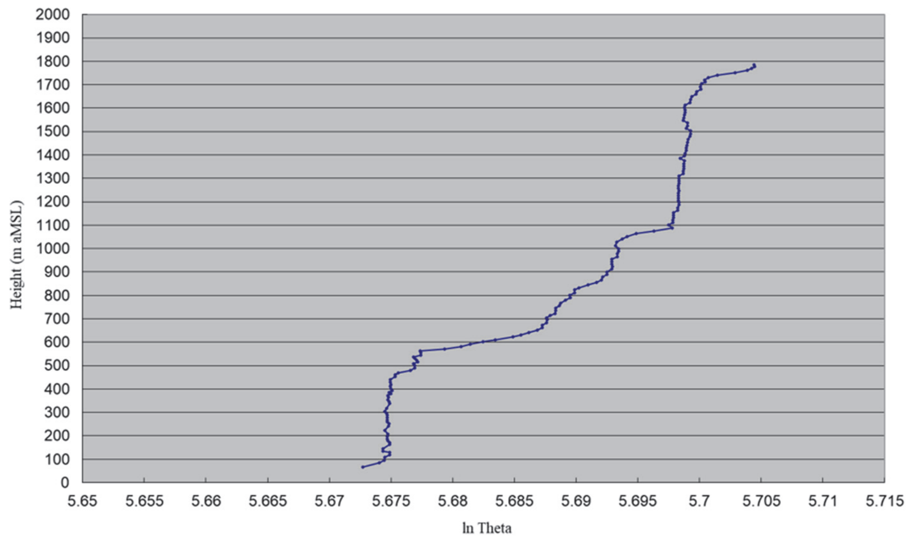

(b)

Fig. 13.(ctd.) Scorer parameter profile (a) and potential temperature profile (b) based on radiosonde data for Lo Fu Tau and the Tung Chung gap.

Simulation has been performed between 21 UTC of January 17, 2026 and 01 UTC of January 18, 2026. In the simulated RHI scans of the LIDAR, mountain waves are clearly observed downstream of Lo Fu Tau (*Fig. 14(a)*) and Tung Chung gap (*Fig. 14(b)*). There is also an extensive area of inbound flow downstream of the mountains of Lantau Island in the simulated PPI scan of the LIDAR (*Fig. 15*). The major features of the LIDAR Doppler velocity scans are reproduced successfully.

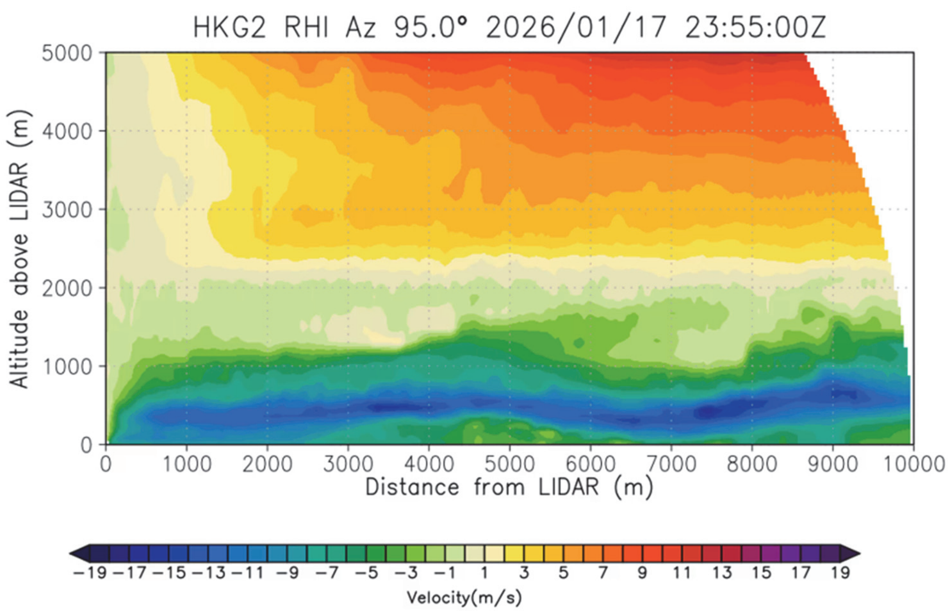

(a)

Fig. 14 Simulated mountain waves at Lo Fu Tau (a) and the Tung Chung gap (b).

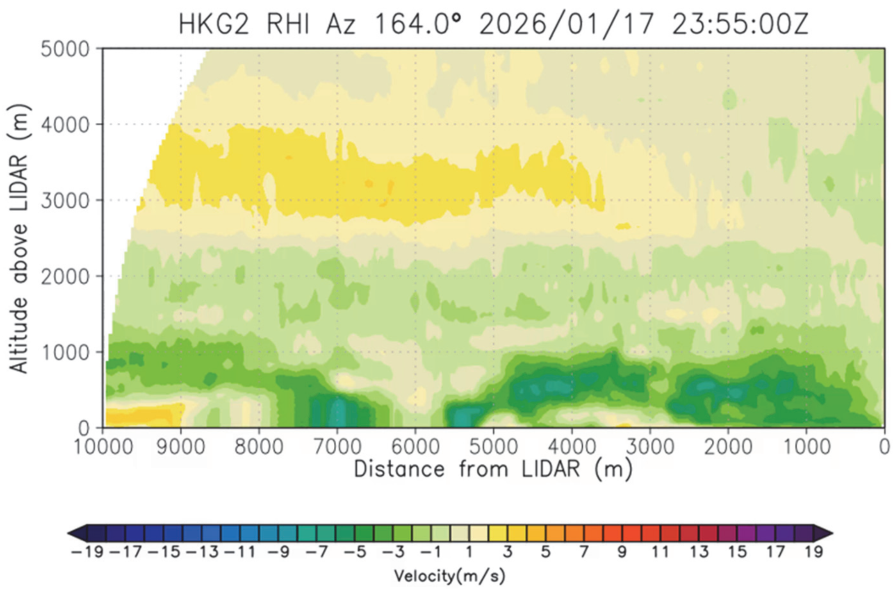

(b)

Fig. 14. (ctd.) Simulated mountain waves at Lo Fu Tau (a) and the Tung Chung gap (b).

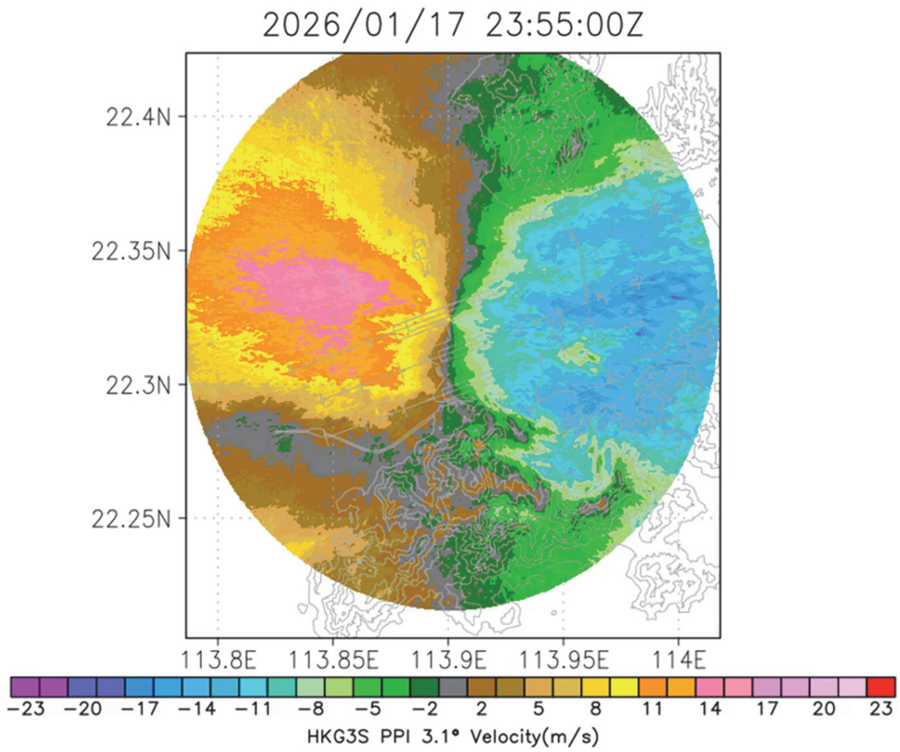

Fig. 15. Simulated PPI scan of HKG3S LIDAR.

4. Conclusion

This paper documents a number of interesting features of terrain-disrupted airflow at HKIA in easterly wind situations. For the first time, vortices associated with KH instability are observed in the RHI scan of the LIDAR. Vortex shedding is observed again, with the period of shedding being analyzed using the wind direction data from a runway anemometer. Jump-like features and mountain waves are also observed in the RHI scans as well. The occurrence of such features is in general consistent with the expectations from the parameters as calculated from the upper air wind and temperature profiles, such as Richardson number, Scorer parameter and Froude number. In addition, this paper suggests that the Scorer parameter could diagnose the background atmosphere favourable for the occurrence of stationary and transient waves at HKIA.

High resolution NWP simulations have been performed to study the possibility of reproducing such features. The simulations are a mixed success. Some features are more readily simulated, such as mountain waves and jump-like features. However, vortices associated with KH instability are not readily reproduced in the simulation. Vortex shedding can be simulated to a certain extent, with the shedding period basically reproduced, but the inbound flow in the vortex does not show up clearly in the simulation. More experiments would be conducted to find out the more appropriate combinations of parameterization schemes in order to be more successful in simulating these flow features.

References

Atkinson, B.W., 1981: Meso-scale Atmospheric Circulations. *Academic Press.* https://doi.org/10.1002/joc.3370020313

Chan, P.W., Lai, K.K., and *Li, Q.S.,* 2021: High-resolution (40 m) simulation of a severe case of low-level windshear at the Hong Kong International Airport—Comparison with observations and skills in windshear alerting. *Meteorological Applications 28,* https://doi.org/10.1002/met.2020

Deardorff, J.W., 1980: Stratocumulus-capped mixed layers derived from a three-dimensional model. *Boundary Layer Meteorology 18,* 495-527. https://doi.org/10.1007/BF00119502

Scorer, R.S., 1949: Theory of waves in the lee of mountains. *Q. J. R. Meteorol. Soc. 75,* 41–56. https://doi.org/10.1002/qj.49707532308

Smagorinsky, J., 1963: General circulation experiments with the primitive equations. *Monthly Weather Review 91,* 99-164. https://doi.org/10.1175/1520-0493(1963)091<0099:GCEWTP>2.3.CO;2

Vosper, S.B., 2000: Three-dimensional numerical simulations of strongly stratified flow past conical orography. *Journal of the Atmospheric Sciences 57,* 3716–3739. https://doi.org/10.1175/1520-0469(2000)057<3716:TDNSOS>2.0.CO;2

White, F.M., 1999: Fluid mechanics (4th ed.). *WCB/McGraw-Hill.* ISBN 978-0-07-116848-9